



**HAL**  
open science

# Structural analysis of a multi-span railway masonry bridge combining in situ observations, laboratory tests and damage modelling

Nathalie Domede, Alain Sellier, Thomas Stablon

► **To cite this version:**

Nathalie Domede, Alain Sellier, Thomas Stablon. Structural analysis of a multi-span railway masonry bridge combining in situ observations, laboratory tests and damage modelling. *Engineering Structures*, 2013, 56, pp.837-849. hal-01743876

**HAL Id: hal-01743876**

**<https://hal.insa-toulouse.fr/hal-01743876>**

Submitted on 26 Mar 2018

**HAL** is a multi-disciplinary open access archive for the deposit and dissemination of scientific research documents, whether they are published or not. The documents may come from teaching and research institutions in France or abroad, or from public or private research centers.

L'archive ouverte pluridisciplinaire **HAL**, est destinée au dépôt et à la diffusion de documents scientifiques de niveau recherche, publiés ou non, émanant des établissements d'enseignement et de recherche français ou étrangers, des laboratoires publics ou privés.

# Structural analysis of a multi-span railway masonry bridge combining in situ observations, laboratory tests and damage modelling

Domede Nathalie<sup>1</sup>, Sellier Alain<sup>2</sup>, Stablon Thomas<sup>3</sup>

<sup>1</sup> Associate Professor, Université de Toulouse; UPS, INSA; LMDC (Laboratoire Matériaux et Durabilité des Constructions); 135, avenue de Rangueil, F-31077 Toulouse CEDEX 04, France, nathalie.domede@insa-toulouse.fr

<sup>2</sup> Professor, Université de Toulouse, alain.sellier@insa-toulouse.fr

<sup>3</sup> PhD, Université de Toulouse, tstablon@etud.insa-toulouse.fr

## ABSTRACT

The paper presents a structural analysis by means of an orthotropic damage model of a multi-span masonry railway bridge built in the early years of the 20<sup>th</sup> century. Its aim is to show how this type of model allows for the current bridge mechanical behaviour under service loads to be assessed and the ultimate load to be forecast. It includes a phase of research on archived documents, an in-situ investigation phase, an experimental phase carried out on core samples in the laboratory, and a computation phase. Among the different calculation steps, a simulation of the bridge history is performed in order to consider the current cracked state induced by support settlement. In a following step, the traffic loads are applied to assess the mechanical behaviour of the bridge under service loads up to failure. The mechanical behaviour of masonry is described by means of an original 3D anisotropic damage model able to consider the opening and the progressive reclosing of localized cracks. The model uses homogenized parameters considering the weakness of the stone-mortar interface. It has the capability to use material pre-damage. The calculation determines the crack pattern induced in the bridge by support displacements and loads. The support displacement study consists of an inverse analysis aimed at determining the actual present state of the structure from the cracking pattern observed on the bridge. The methodology highlights the importance of considering the whole history of a masonry structure when assessing the current state.

Keywords: Masonry bridge, assessment, damage model, crack opening, FEM, homogenization

## Introduction

This paper presents a structural analysis of a multi-span masonry railway bridge built in 1904 near Paris. The purpose of the research was to create a calculation tool, based on an anisotropic damage mechanical model with crack reclosing functions, able to assess the 3D mechanical behaviour of old masonry structures, in particular cracked stone bridges affected by support displacements. The model is used in a global methodology intended to assess the strains under service loads and to evaluate the ultimate load of the bridge. The requirement considered was that the tool had to be usable by practitioners on most masonry railway bridges.

According to Orbán and Gutermann [1], about 50% of all railway bridges in Europe consist of masonry arches. These bridges are old (more than a hundred years old) and traffic is increasing. Disorders, cracks and sometimes collapses, occur. That is why research programmes to create engineering tools have been developed in several European countries in the past forty years or so. They were initially based on limit analysis theory, with programs such as ARCHIE in Scotland, VOUTE in France (1980's) and RING in England (1990's), then used a Finite Element Method or Distinct Element Method (see Proske and Van Gelder [2] for a review of the history of masonry bridge calculation). Research on the topic is continuing in several laboratories in Europe with different approaches: elastic formulation, limit analysis, and elasto-plastic or

damage analysis at macro, meso or micro scales. A review of the methods applicable to the study of historical masonry constructions is given by Roca *et al.* [3].

In the special case of masonry railway bridges, Orbán developed a global assessment method using non-destructive investigation and non-destructive in-situ load testing. Helmerich *et al.* [4], at Wroclaw University, combined non-destructive testing and elasto-plastic analysis of the structure. In their work, the masonry arch barrel is modelled with a meso approach, considering two types of materials: masonry blocks as a linear elastic isotropic material, and mortar joints, as a plastic concrete-like material. The backfill is a granular soil (Drucker Prager model) separated from the arch barrel by contact elements. In the masonry arch, predefined planes of weakness are located in the mortar joints. The results are given as maps of plastic strains and ultimate load. At the University of Toulouse, a research programme carried out with SNCF (the French railway company) in the aim of assessing masonry railway bridges, has been in progress for ten years and includes destructive tests (coring), in-situ tests (measurements with video cameras and LVDT) and the creation of a computation tool based on FEM. This work on old masonry arches focuses on the emergence of cracking, in 3D, by means of the anisotropic damage theory coupled with plasticity, in order to determine the displacements of the structure and the zones where it is damaged. No weak zones are defined in advance, which significantly simplifies the mesh of the structure as it depends only on geometrical considerations. The final aim is to assess the current behaviour under service loads and to forecast the ultimate loads.

In the research presented here, the mechanical behaviour of the masonry is described using a continuum damage model applied at the macro scale with material parameters assessed by means of a homogenization method. It considers the elastic and inelastic domains. With this damage model, initially developed by Sellier *et al.* [5][6][7] for concrete and adapted for masonry [8], cracks can appear anywhere in the bridge and propagate in any direction, in both tensile and compressive zones, then possibly reclose depending on the stress state. The efficiency of this model in describing masonry mechanical behaviour was presented in 2010 [8]. Since then, improvements have been made. In the present paper, general aspects of the methodology previously presented at the SAHC12 conference [9] are recalled. However, the main purpose here is to describe how the initial damage induced by the displacement of the supports or by the building process can be considered in the calculations, thanks to the numerical model and the in-situ-investigations. The method consists of explaining the crack pattern observed in situ through a parametric study of the support displacements. The bridge behaviour then depends largely on the progressive restitution of stiffness during reclosing of these cracks when a service load is applied.

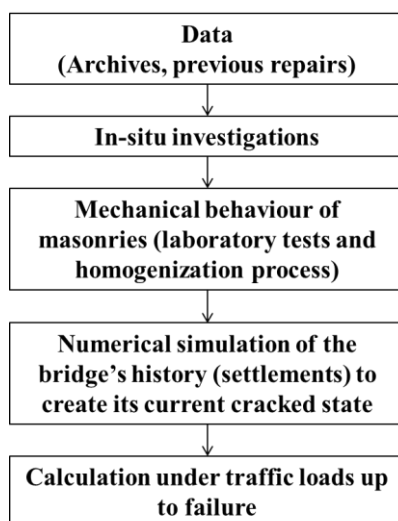


Fig. 1. Global analysis method for a masonry bridge

Obviously, the current behaviour of the masonry depends not only on the crack reclosing process but also on the constitutive behaviour laws of uncracked zones. These were assessed by means of laboratory tests on core samples drilled in the different materials of the bridges (different stone types and mortar). Once the individual behaviour laws were known, they were combined by means of a homogenization method to give the mean behaviour per masonry zone. Block-mortar interface pre-damage also had to be considered in the model since, as noted by Stablon *et al.* [10], the history of the building process sometimes explains the weakening of the stone-mortar interface.

Finally, because of the major influence of existing cracks in the structure, the global mechanical behaviour of an old masonry bridge is strongly dependent on its history, including the initial building process and subsequent movement of the supports, which governs its current stiffness. To consider this last aspect, in-situ measurements of crack openings and vault displacements under train loads had to be made.

The work presented here includes a case study carried out on a long, multi-span stone masonry bridge (description in section 2). The methodology is summarized in Fig.1. Relevant values and results of calculations were compared in order to fit the support settlements explaining the crack pattern, itself explaining the current masonry stiffness. A realistic calculation of the bridge was thus possible under service load, then up to ultimate loads. The results of this study are given in the third section.

## 1. The mechanical behaviour model

First, it is essential to specify that the non-linear model used for the bridge calculations is a macroscopic one, so it employs only homogenized material parameters. In fact, even if each zone of the bridge is made up of several materials (stones and mortar), the homogenized behaviour law has to be determined for each zone before the bridge analysis can be carried out. Once the homogenized behaviour law is known, a damage model is used to consider the cracking and the crack reclosure possibilities. The macroscopic model is presented first, followed by the homogenization technique and associated experimental tests.

The calculation process based on the damage model determines the location and orientation of the main cracks that may develop in all directions in 3D, regardless of the mesh. These cracks can open, reclose and intersect. The masonry cracking state is then described by an orthotropic damage tensor. The damage model was first described by Sellier for concrete structures and the crack reclosure possibility was added recently, on the basis of Jefferson's works [11]. Its adaptation to masonry structures was first successfully investigated by Stablon [12]. This section recalls the main principles of the damage model and its particularities concerning the gradual crack reclosure it allows. Then it focuses on the adaptations proposed for the case of old masonry vaults.

### 1.1 General presentation of the model

The model uses an orthotropic Rankine multi-criterion in tension to consider localized crack propagation perpendicularly to the main direction of tension, and an isotropic Drucker Prager criterion to consider shear and compression failures. The need to combine Rankine and Drucker Prager criteria has already been studied by several authors for concrete structure modelling [13][14][15][16][17]. A comparative study of these models can be found in [18]. However anisotropic models have rarely been used for masonry structures. Lishak *et al.* [19] used the damage mechanics to model two-dimensional masonry walls. Here, in the case of massive masonry bridges in which a crack can propagate longitudinally, transversally or crosswise, a 3D damage formulation is needed. With the 3D damage model used here, the initiation, propagation

and widths of cracks are determined according to local strain, without any initial assumptions on crack location or orientation, in contrast to the technique used in discrete element or joint element based models. So, the cracks and damage zones are consequences of the strain localization process induced by the softening phase of the behaviour law. The model is based on the “effective stress-equivalent strain” concept developed by Lemaitre *et al.* [20]. In the following presentation of the main equations, the stress and strain symmetric tensors are substituted by their six component pseudo vectors for reasons of convenience, as in FEM. In this model, the effective stress  $\overset{K}{\sigma}$ , is calculated according to (1):

$$\overset{K}{\sigma} = \mathbf{S}_0 \cdot \overset{K}{\varepsilon} \quad (1)$$

This stress corresponds to the “idealized” undamaged part of the material. In (1),  $\overset{K}{\varepsilon}$  is the elastic strain and  $\mathbf{S}_0$  is the stiffness matrix of the healthy (undamaged) material. The stress  $\overset{K}{\sigma}$  is then separated, by a principal stress decomposition method, into a negative part  $\overset{K}{\sigma}_c$  in compression, and a positive part  $\overset{K}{\sigma}_t$  in tension (2).

$$\overset{K}{\sigma} = \overset{K}{\sigma}_c + \overset{K}{\sigma}_t \quad (2)$$

The internal variables that characterize the damage state of the masonry are the damage tensor  $\mathbf{D}_t$  in tension, and the scalar damage  $D_c$  in compression. In tension, Rankine orthotropic criteria are used in a rotating crack framework [7]. The main effective tensile stresses are used to update a Rankine stress tensor which memorizes the maximal effective tensile stresses endured by the material. Crack rotation occurs when an effective tensile stress acts in a direction different from the previous main direction of this tensor. The model was successful in various benchmark tests often used on concrete damage models. It performed successfully in, among others, the Willam test concerning the ability to manage a rotation of the main damage direction, as discussed in [17][21] (results available in [7]). The main advantage of the orthotropic formulation of tensile damage is, as explained below, to facilitate localized crack reclosure management. The Rankine Criterion (Maximal Tensile Stress criterion, also called MTS by Erdogan and Sih [22]) is often used to model damage or plasticity in brittle materials. In the present model, the main values of the damage tensor ( $\mathbf{D}_t$  main values) are computed according to an evolution law based on experimental results, which is compatible with the second principle of the thermodynamics [20]. As illustrated in Fig. 2, the behaviour law presents a softening phase. The independence of the fracture energy with respect to the finite element size is ensured through an anisotropic Hillerborgh method [23] able to consider finite elements with anisotropic geometries [7][10]. This particularity of the model is clarified below.

In compression, the negative part  $\overset{K}{\sigma}_c$  of effective stresses is used to assess a Drucker Prager equivalent stress  $\sigma_{DP}$  (3), on which the damage variable  $D_c$  depends. The damage evolution law is also chosen in accordance with experimental results and thermodynamic principles. It includes a Hillerborgh method to control the energy dissipated during softening [6].

$$\sigma_{DP} = \sqrt{\frac{J_{2d}}{6}} + \delta \frac{I_1}{3} \quad (3)$$

where  $J_{2d}$  is the second invariant of the deviator of  $\overset{K}{\sigma}_c$ ;  $I_1$  is the trace of  $\overset{K}{\sigma}_c$ ;  $\delta$  is the Drucker Prager constant, which depends on the internal friction angle  $\varphi$  as follows in (4).

$$\delta = \frac{2\sqrt{3} \sin \varphi}{3 - \sin \varphi} \quad (4)$$

Once the damages are known, they influence the effective stress  $\overset{\mathcal{K}}{\sigma}$  (6). They allow crack reclosure to be included in the mechanical formulation, through the effective stress in the localized cracks  $\overset{\mathcal{K}}{\sigma}_f$  given in (5). The apparent stress  $\overset{\mathcal{K}}{\sigma}$  to be used at integration points of the finite element code is obtained by (6), where  $\mathbf{1}$  is the identity tensor.

$$\overset{\mathcal{K}}{\sigma}_f = \overset{\mathcal{K}}{\sigma} - \overset{\mathcal{K}}{\sigma}_{pl} \quad (5)$$

$$\overset{\mathcal{K}}{\sigma} = (1 - D_c) \cdot ((\mathbf{1} - D_t) \cdot \overset{\mathcal{K}}{\sigma} + D_t \cdot \overset{\mathcal{K}}{\sigma}_f) \quad (6)$$

In (5),  $\overset{\mathcal{K}}{\sigma}_{pl}$  is a plastic stress following a crack reclosure yield function described in [6]. It is equal to  $\overset{\mathcal{K}}{\sigma}$  during the tensile damage process. Thus, the stress in the localized cracks  $\overset{\mathcal{K}}{\sigma}_f$  is zero until a crack reclosure is activated. Details of the reclosure process modelling are given in [6]. The advantage of using an orthotropic damage tensor is the possibility it provides to activate crack reclosure in a single direction, without modifying the stress in the two orthogonal cracks. In a masonry structure, this possibility is important since several cracks can coexist in the same element because of the complex loading history. For example, a support displacement can create a transversal crack under the vault and, later, a large load on the bridge can create a longitudinal crack in the same finite element.

The behaviour law of the material under uniaxial loading is represented in Fig. 2.

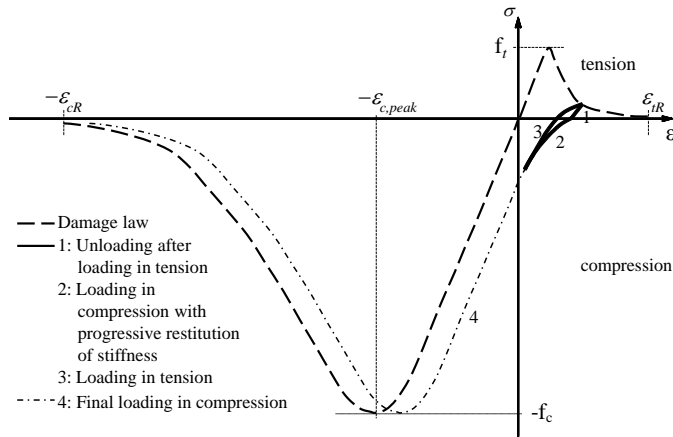


Fig. 2. Damage model, behaviour under cyclic axial loading (cycle order numbers 1 to 4).

In Fig. 2, the strengths are noted  $f_c$  in compression and  $f_t$  in tension, and the peak strain in compression is  $\varepsilon_{c,peak}$ . Before damage, the law is characterized by a same elastic modulus in uniaxial compression and tension, noted  $E$ . These 4 parameters ( $f_c, f_t, E, \varepsilon_{c,peak}$ ) have to be determined experimentally or by a homogenization technique if the damage model is applied to a sizeable zone of masonry including stones and mortar joints.

As illustrated in Fig. 2, the damage evolution law leads to a post-peak softening phase in relation with the fracture energy in tension  $G_t$  and in compression  $G_c$ . To avoid a dependence of the finite element solution on the mesh size, the Hillerborgh method imposes that the damage

evolution law must depend anisotropically on the finite element size. For an eight-node cubic element, the element length is assessed by (7).

$$l_I = \frac{2}{\left\| \overline{J}^{-1} \cdot \underline{\underline{e}}_I \right\|} \quad (7)$$

In (7),  $\underline{\underline{e}}_I$  is a main direction of the Rankine effective stress tensor,  $\overline{J}^{-1}$  is the inverse of the Jacobian Matrix corresponding to the geometric transformation between the reference finite element and the real ones.

An anisotropic Hilleborgh method allows the structure to be meshed independently of the forecast cracking pattern. An anisotropic volume cracking energy  $g_t$  (or  $g_c$ ) is then used ((8) and (9)), depending on the orientation of the crack, and chosen in such a way that the energy under the tensile curve equals  $G_t$  (or  $G_c$ ) whatever the size of the element (noted  $l_I$ ) in the direction perpendicular to the crack, i.e. in the main direction “I” of the stress tensor.

$$G_t = g_t \times l_I \quad (8)$$

$$g_t = \frac{f_t^2}{2E} + \int_{\varepsilon_{t,peak}}^{\varepsilon_{tR}(l_I)} E(1 - D_{tI}) \varepsilon d\varepsilon \quad (9)$$

The model also supplies the Crack Mouth Opening Displacement (*CMOD*). It is calculated directly at the Gauss point during the finite element solving procedure. *CMOD* depends both on the damage state and on the strain state. In the present model, it corresponds to the average crack opening displacement computed assuming a single localized crack in each direction of an element damaged in tension. It is approached using (10) in the main direction of the Rankine effective stress “I”. It is convenient for practitioners to have the *CMOD* to compare the value supplied by the finite element code with those measured in situ. Another advantage is to manage the crack reclosure directly in terms of *CMOD*, instead of strains, as explained below.

$$CMOD = l_I \cdot \left( \frac{\tilde{\sigma}_{tI}}{E} \right) \cdot \left[ \frac{D_{tI} - D_{t,peak}}{1 - D_{t,peak}} \right] \cdot H \left( \frac{D_{tI} - D_{t,peak}}{1 - D_{t,peak}} \right) \quad (10)$$

In (10),  $D_{tI}$  is the tensile damage value in the main direction I;  $D_{t,peak}$  is the damage value at peak tension;  $\tilde{\sigma}_{tI}$  is the current value of the tensile effective stress in the main direction I;  $H$  is the Heaviside function defined by  $H(X) = 1$  for  $X > 0$ , 0 otherwise.

(10) assumes that *CMOD* becomes equal to the displacement at the edges of the “cracked” finite element when the tensile damage  $D_{tI}$  tends to 1. It also assumes that the localization starts at the peak of the tensile law behaviour  $D_{t,peak}$ . Another advantage of using this variable to complement the classic damage variable is the fact that, even if many limited cracks occur in a massive structure, only the main cracks will stay open until failure and all the surrounding ones will be reclosed. *CMOD* is then able to capture this main crack among the multiple damaged elements. This ability of the model is described in [6]) for crack propagation in a concrete element.

To describe the progressive restitution of stiffness in compression during the crack reclosing process (step 2 in Fig.2), the model introduces a specific parameter, noted  $w_{ref}$ . This parameter allows the roughness of the crack edges to be taken into consideration. The effective stress in the direction “I” perpendicular to the crack is given by (11).

$$\tilde{\sigma}_{fI} = -f_t \frac{w_{ref}}{CMOD + \alpha w_{ref}} \quad (11)$$

where  $\alpha$  has a value close to zero, arbitrarily chosen to prevent division by zero when the crack is subjected to high compression. The behaviour of a crack corresponding to this equation is illustrated in Fig. 3.

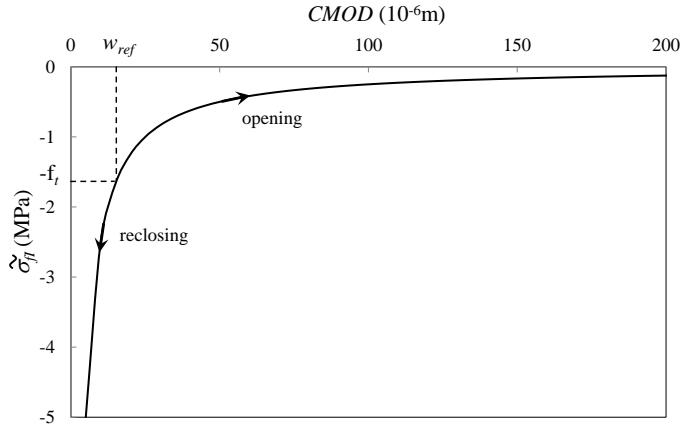


Fig. 3. Crack reclosure function (stress in the crack vs. crack opening)

When a crack reclosure is activated, as illustrated for the loading pass 1-2-3 in Fig. 2, a uniaxial plastic flow is activated. The curve in Fig. 3 then corresponds to the evolution of the yield function associated with this plastic flow. The advantage of the orthotropic formulation is to have a different yield function for each of the three possible cracks that can coexist in a finite element. Another advantage is linked to the fact that crack reclosure have to be managed in terms of  $CMOD$  (and not strains). The  $CMOD$  is independent of the finite element sizes thanks to the anisotropic Hillerborgh method, which regulates the mesh dependency accurately.

To finish the presentation of this model, it is necessary to recall that, as  $CMOD$  and the damage are the internal variables of the model, they can be initialized to non-zero values in order to consider possible pre-damage to the masonry. In the next section, this possibility is exploited to adapt the model to old masonry.

## 1.2. Application to old masonry

### 1.2.1 Pre-damage

The main adaptation of the model to old masonry consists of considering the fact that an old masonry structure is pre-damaged in its current state. Furthermore, at the very beginning of the loading, the experimental curves in compression show a progressive increase of the stiffness until the Young's modulus  $E$  is reached. This phenomenon comes from the fact that the material contains initial cracks that reclose in compression. These initial cracks characterize calcareous rocks, and, in the case of masonry structures, also result from the initial building process as shown by Stablon *et al.* [10]. In masonry structures, the shrinkage of the mortar joints between the stones, at construction time, creates pores and cavities that weaken the masonry.

These experimental results are considered in the model by means of initial pre-damage  $D_{t0}$ . The behaviour law taking this pre-damage into account is illustrated in Fig. 4.

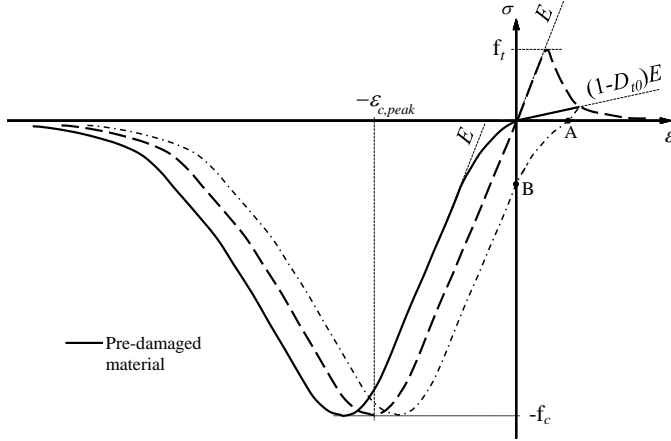


Fig. 4. Comparison between the healthy material and the pre-damaged material

As the thermodynamic conditions require an increase of  $D_{II}$ , condition (12) is always satisfied by the model, ensuring that the calculated damage is always greater than the imposed pre-damage.

$$\mathcal{D}_{II} \geq 0 \quad (12)$$

When initial damage is imposed in an element, the model automatically calculates the initial Crack Mouth Opening Displacement  $CMOD_0$  given in (13), corresponding to a material free of stresses. This relation is the consequence of (10) and (11). It means that if damage exists, an associated non-zero  $CMOD$  has existed before, and, due to the plastic flow rules, a plastic  $CMOD$  remains since the material was unloaded. The point A in Fig. 4 is then the new initial material state. If this point is shifted to zero, the behaviour law obtained seems to present a curvature inversion at the beginning of the compressive loading. In fact, this curvature inversion is the consequence of a crack reclosure.

$$CMOD_0 = l_I \sqrt{\frac{f_t w_{ref} D_{t0}}{l_I E}} \quad (13)$$

(14) gives the initial plastic stress  $\tilde{\sigma}_{pl}$  in the crack. This plastic stress is considered in (5) and (6) to model the curvature inversion.

$$\tilde{\sigma}_{pl} = f_t \frac{w_{ref}}{CMOD_0} \quad (14)$$

To summarize: if the first stress applied to the pre-damaged material is a compression, it will first be necessary to reclose the crack. In this way, the initial compaction phase of cracked materials (observed during tests) is modelled.

### 1.2.2. Homogenization

In a macro approach, the behaviour law uses homogenized parameters to represent the mechanical behaviour of the composite material, from the healthy state without any cracks, or pre-damaged state, up to failure. In cases of existing masonry, as it is often impossible to take a

representative volume of the various components from the bridge, but only core samples drilled in different materials, a numerical homogenization process has to be used to determine the mechanical parameters of the behaviour law of a masonry representative volume.

The aim of this paragraph is to explain how the 10 homogenized parameters involved in the model (6 in compression:  $E$ ,  $\nu$ ,  $f_c$ ,  $\epsilon_{c,peak}$ ,  $G_c$ ,  $\delta$ , and 4 in tension:  $f_t$ ,  $G_t$ ,  $w_{ref}$ ,  $D_{t0}$ ) are determined.

#### *Homogenization in compression*

There are two steps in the method: the first is experimental, the second is numerical. It is summarized in Fig. 5. First, the mechanical parameters of each component of the masonry are determined separately. This begins by a characterization of the elementary material (stones on one side, mortar on the other) by means of displacement controlled compression tests.  $E$ ,  $\nu$ ,  $f_c$  are the mean values of these tests results. The values of  $\epsilon_{c,peak}$  and  $G_c$  are fitted on experimental curves. The tensile strength is measured using split tests.

The compression strength of the mortar embedded between two pieces of stone increases due to the confinement effect, which acts in the Drucker Prager criterion through the parameter  $\delta$ . It is assessed by means of compression tests carried out on multilayer samples (stone-mortar-stone) extracted from masonry, so that the interface is not altered. The value of  $\delta$  is chosen so as to recover the experimental stress-strain curves with a FEM simulation.

The individual parameters are introduced into a numerical calculation of a masonry representative volume, as suggested in a previous study presented at SAHC10 [24]. This homogenization method uses the damage model described above to consider each elementary phases of the masonry at this scale, but other models could also be used successfully.

For the homogenization in compression, a representative elementary volume (REV) of masonry is computed numerically, considering each individual material with its own characteristics given by the tests. The REV chosen is a numerical wall, the dimensions of which are defined for “real tests” in the European standard specifications (EN 1052-1, 1999). The wall is loaded by applying a vertical displacement inducing compression and transverse tensions in the composite wall. The parameters of the homogenized masonry damage law are then fitted. This step provides the elastic moduli, the compressive strength, the Poisson’s ratio, the strain at peak and the fracture energy of the masonry, in compression. The parameter  $\delta$  is not modified.

#### *Homogenization in tension*

The homogenized non-linear law is controlled by the stone-mortar interface, since it is the weakest zone of the stone masonry. Kim *et al.* [25] confirmed recently that interface debonding occurs before the blocks crack. Therefore, it is assumed that the softening branch of the masonry behaviour in tension is that of the mortar-stone interface. The behaviour of the interface is measured by means of 3-point bending tests, carried out on special samples with an interface in the middle. Then, the analysis of load-displacement curves gives the fracture energy in tension, the tensile strength, and the pre-damage  $D_{t0}$ .

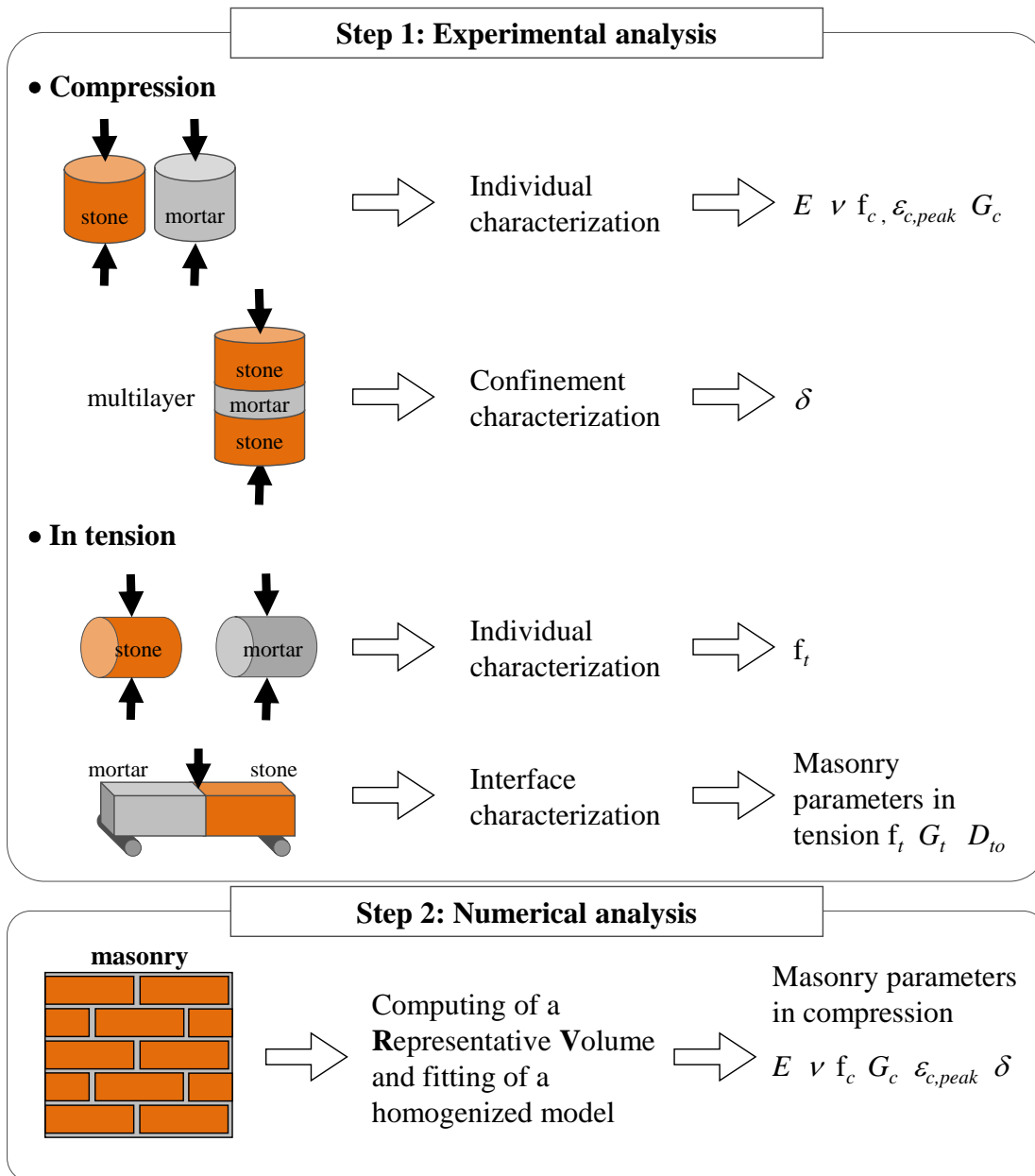


Fig. 5. Individual material characterization (step 1) and homogenization method principles (step 2)

## 2. The bridge under study

### 2.1. Description

The bridge studied (Fig. 6) was a stone masonry viaduct built in 1904 (9 spans, total length 136m) in the close neighbourhood of Paris. Traffic on the two railway lines is very intense and the bridge is subjected to the repeated passage of suburban passenger trains and freight trains, with 80 to 150 crossings daily.

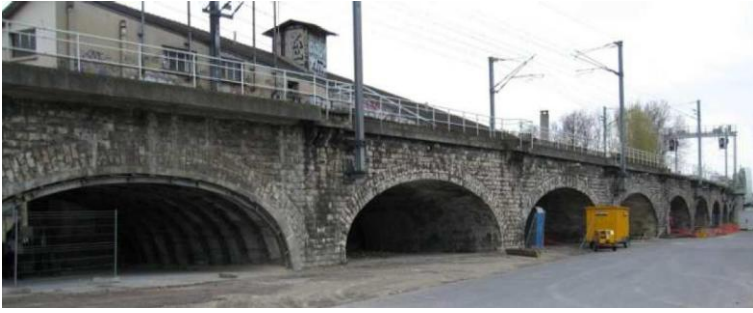
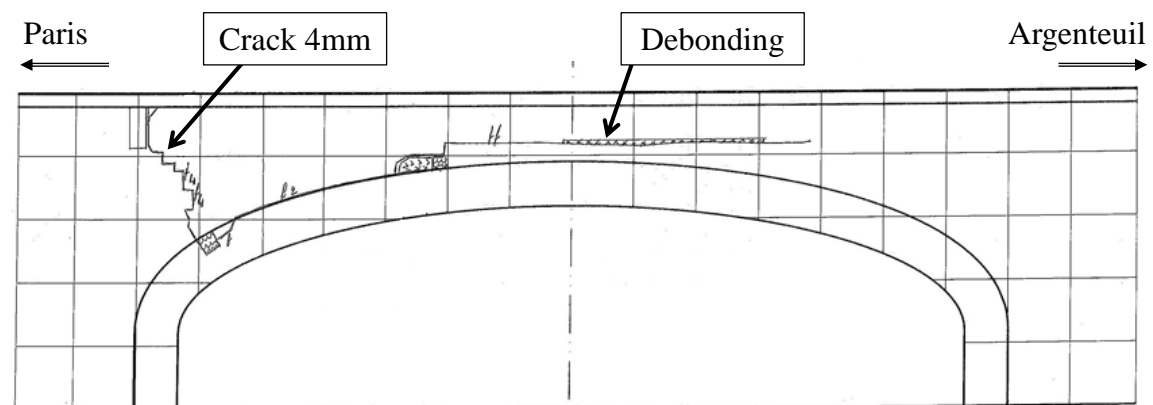
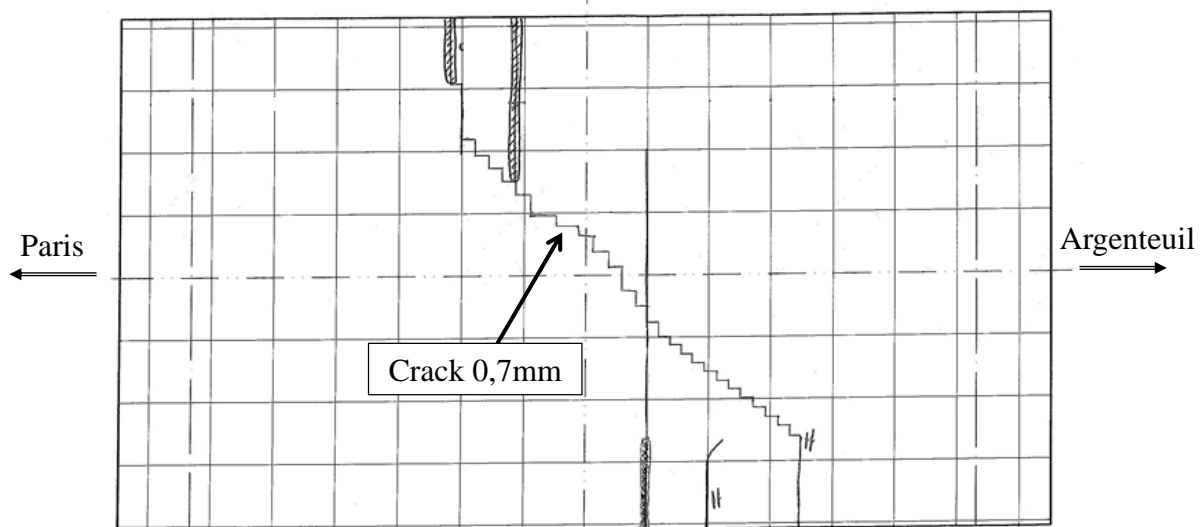


Fig. 6. The masonry bridge studied (9 spans about 12.5 m long, 8m wide)

Disorders have appeared on this bridge: displacements of foundations, and transversal, longitudinal and skew cracks in the third span (Fig. 7). The bridge has been reinforced by adding steel arches under some of the original arches of the viaduct (no reinforcements in the third span). Concrete and steel micro-piles were installed beside the original timber piles in 2008. Cracks can still be seen on the spandrel wall and in the intrados of the vaults. They most often pass through the mortar joints between the stone blocks (especially longitudinal and skew cracks under the intrados) but sometimes through the stones themselves.



View from under the intrados



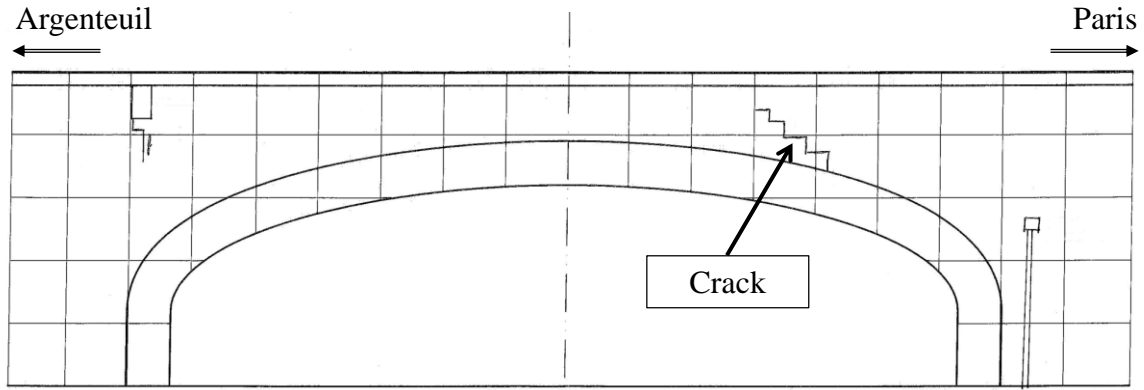


Fig. 7. Disorders in third span, side views from the north and the south, and longitudinal view under the intrados [12].

## 2.2. Measurement of displacement and crack opening under service loads

All the measurements were made in the third span, while a freight train was crossing the bridge. They included:

- Measurement of relative and absolute deflection under the intrados at mid span,
- Measurement of horizontal and vertical displacement at the 4 points shown on Fig. 8,
- Measurement of width of cracks (precision  $10 \cdot 10^{-6} \text{m}$ ).

At the same time, the train weight, temperature and relative humidity were noted.

These investigations showed that the axle loads varied from 115 to 133kN, and the deflection reached a maximum value of 0.33mm. The mean value of the vertical displacement under the freight train was 0.22mm. The opening variation of the cracks was negligible under the train load.

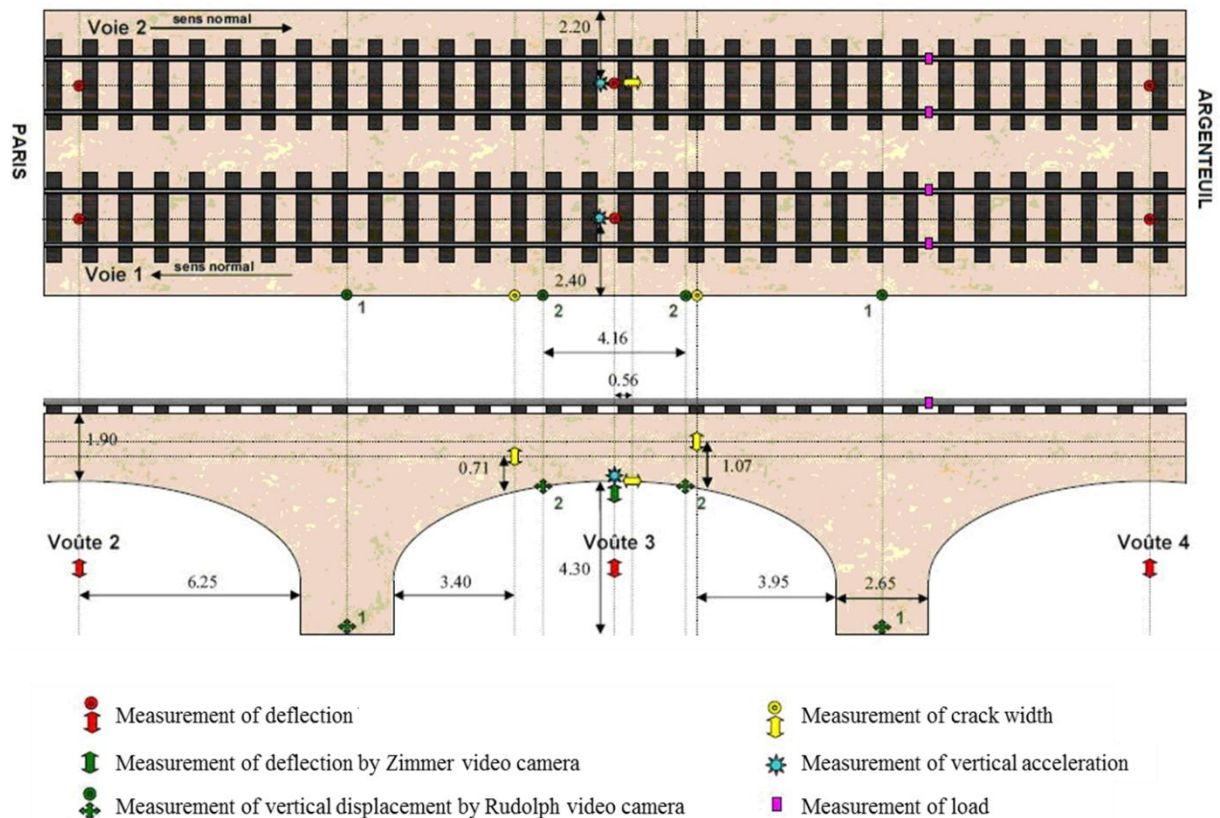


Fig. 8. In-situ measurements on the third span of the bridge [16]

### 2.3. Extraction of cores from the masonries

In July 2008 and January 2009, 5 cores were extracted from the bridge, in the third span, from under the intrados of the vault. The cores were 0.7 to 1.20m long, with a diameter of 9.5cm (Fig. 9).

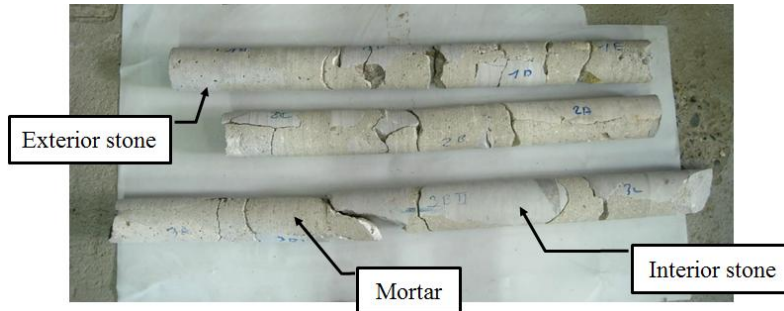


Fig. 9. Cores extracted from under the 3<sup>rd</sup> span.

Examination of the cores showed that there were 2 types of stone in this masonry bridge: a beige exterior calcareous stone (at left on the photo) and a grey calcareous stone for interior masonry (at right on the photo). The mortar linking the stone blocks consisted of small and large aggregates. In these cores, small samples were extracted from each of the 3 components to determine their individual properties, and from the mortar above the mortar-block joints to determine its behaviour when embedded between two stone blocks. The behaviour of the mortar-stone interface was also investigated, as described below.

## 3. Laboratory tests and homogenization process

The homogenization processes had to be carried out for each of the three main zones of the bridge:

- Zone 1: vault and spandrel wall composed of “exterior” stone and mortar
- Zone 2: internal masonry composed of “interior” stone and mortar
- Zone 3: internal fill.

### 3.1. Individual mechanical characteristics of stones and mortar

The mechanical parameters of each component of the masonry (stones, mortar, and mortar-stone interface) were determined separately by means of an experimental procedure (Fig. 5, step 1). Both types of stone were calcareous, homogenous and isotropic.

The characteristics of the materials are given in Tab. 1. The Poisson coefficient ( $\nu$ ), the Young's modulus ( $E$ ), and the compressive strength  $f_c$  are the mean values of the results of uniaxial compression tests as defined in EN14580 ( $\nu$  and  $E$ ) and EN1926 ( $f_c$ ) (6 samples of interior stone, 2 samples of exterior stone, and 8 samples of mortar). The split tensile test (NFP94-422-5) gave the mean value of the tensile strength  $f_t$  (4 samples of each material). Fig. 10 compares the behaviour of stones in compression with model (Fig. 10.1 and Fig. 10.2) and the behaviour of mortar in compression (Fig. 10.3). The values of the fracture energy in compression  $G_c$  and strain at peak  $\varepsilon_{c,peak}$  are fitted on these curves.

Without experimental results able to provide cracking energy in tension, the authors calculated  $G_t$  using (15), valid for geomaterials, where  $l_c$  is the characteristic length of the sample, i.e. 10 cm. This formula gives an approximate value within 20%.

$$G_t = l_c \frac{f_t^2}{E} \quad (15)$$

Table 1.

Parameters used for individual materials

\*only one experimental value; \*\* only 2 experimental values; the coefficient of variation is indicated in brackets (%).

Material	$\nu$	$E$ (GPa)	$f_c$ (MPa)	$\varepsilon_{c,peak}$ (mm/m)	$G_c$ (MJ/m <sup>2</sup> )	$f_t$ (MPa)	$G_t$ (MJ/m <sup>2</sup> )
Interior stone	0.26*	76(6)	172(8)	3.7	0.11	8(18)	$7 \cdot 10^{-5}$
Exterior stone	0.25*	39**	120**	3.8	0.07	10**	$2 \cdot 10^{-4}$
Mortar	0.19 (18)	5(4)	17(5)	4.8	0.02	1.2(17)	$2 \cdot 10^{-5}$

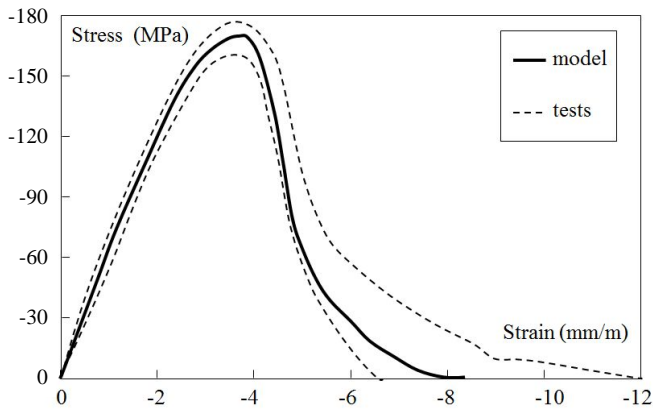


Fig. 10.1. Compression behaviour law for interior stones - tests and model

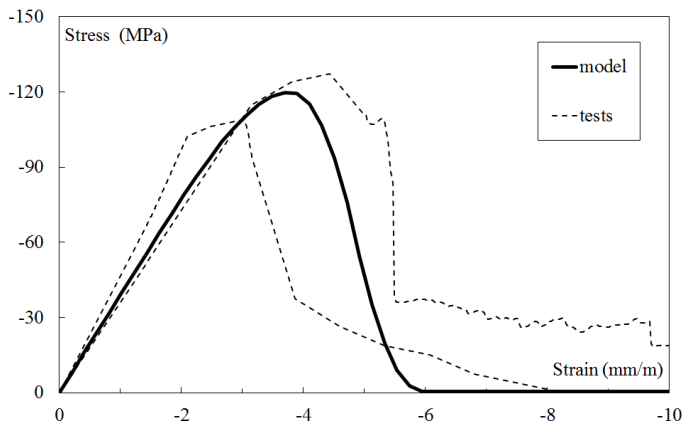


Fig. 10.2. Compression behaviour law for exterior stones - tests and model

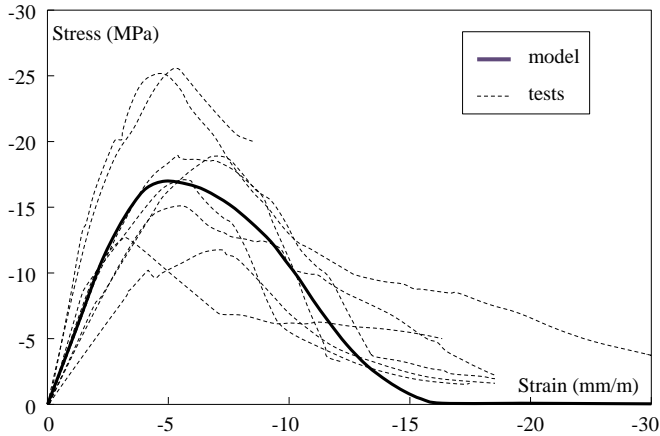


Fig. 10.3. Compression behaviour law for mortar - tests and model

### *Experimental characterization of the confinement effect of mortar*

This was achieved by means of compression tests on stone-mortar-stone multilayers. Nine uniaxial compression tests were carried out on cylindrical cores (diameter 2.65cm, height 6.6cm to 9.25cm) including mortar embedded between two pieces of stone (Fig. 11). The failure of the sample resulted from failure of the mortar when the mortar width was large relative to that of the stone but from failure of the stone (axial crack) when the mortar width was small, because of the confinement effect applied to the mortar joint by the bonded stone blocks. Thus, these tests gave the effect of confinement on mortar. A numerical inverse analysis of these tests determined the confinement parameter  $\delta = 0.52$  (relative to an internal friction angle  $\varphi = 23^\circ$ ).

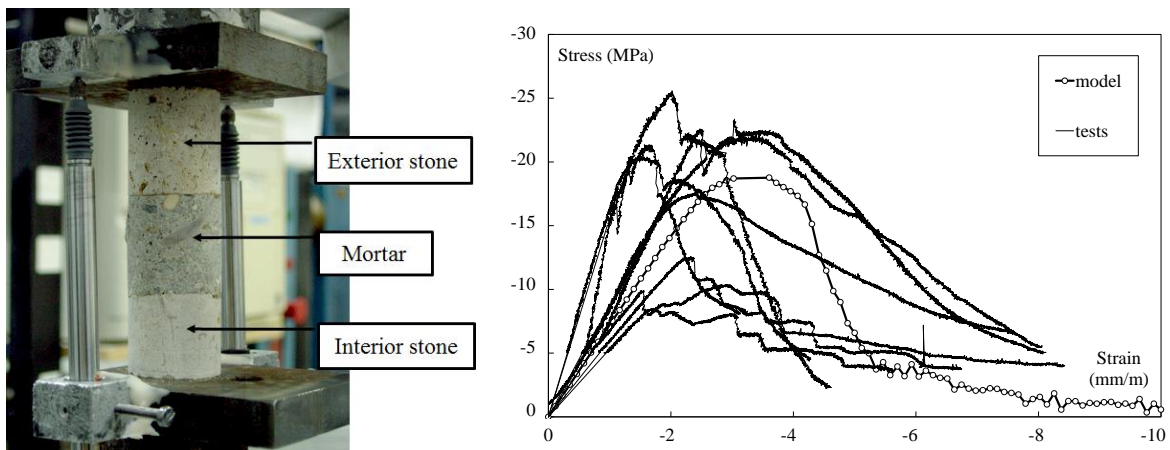


Fig. 11. Compression tests on composite sample. Comparison between tests and model.

## *3.2. Homogenization*

### *3.2.1. In compression*

The mortar and stone composite behaviour was assessed by calculating a representative elementary volume as explained in section 2.3. We obtained the parameters given in Tab. 2. (The dimensions of the stone blocks were 40cm x 25cm x 30cm. The mortar joint thickness was 2cm). Fig. 12 compares mortar behaviour in compression, exterior facing stone behaviour, and the homogenized behaviour law for the masonry.

Table 2

Parameters of homogenized behaviour law for masonry in compression

Masonry	$\nu$	$E$ (GPa)	$f_c$ (MPa)	$G_c$ (MJ/m <sup>2</sup> )	$\epsilon_{c,peak}$ (mm/m)
Interior stone	0.25	41	116	0.10	3.8
Exterior stone	0.25	27	84	0.06	4.0

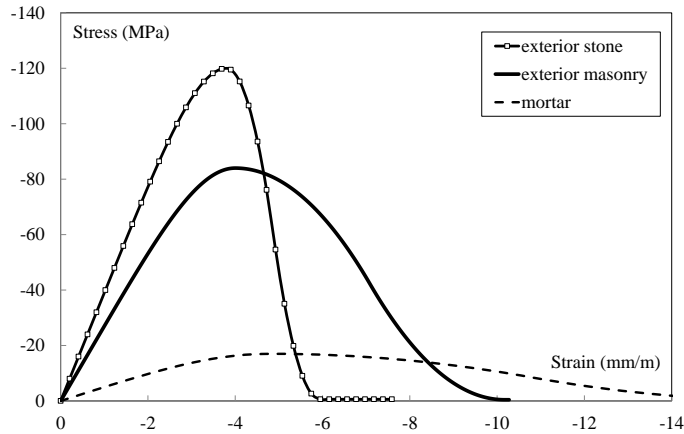


Fig. 12. Compression behaviour law for exterior stone masonry: comparison between mortar, stones and homogenized masonry models.

### 3.2.2. In tension

The homogenized behaviour was the same as in compression for elastic properties but, for the non-linear phase, only the mortar-stone interface was considered. Six 3-point-bending tests were carried out on special samples made of a mortar joint embedded between 2 pieces of stone as can be seen in Fig. 13 (displacement increasing by 0.01mm/min). The numerical inverse analysis of these tests gave the pre-damage  $D_{t0}$  of the stone-mortar interface. The law adopted is shown in Fig. 13.

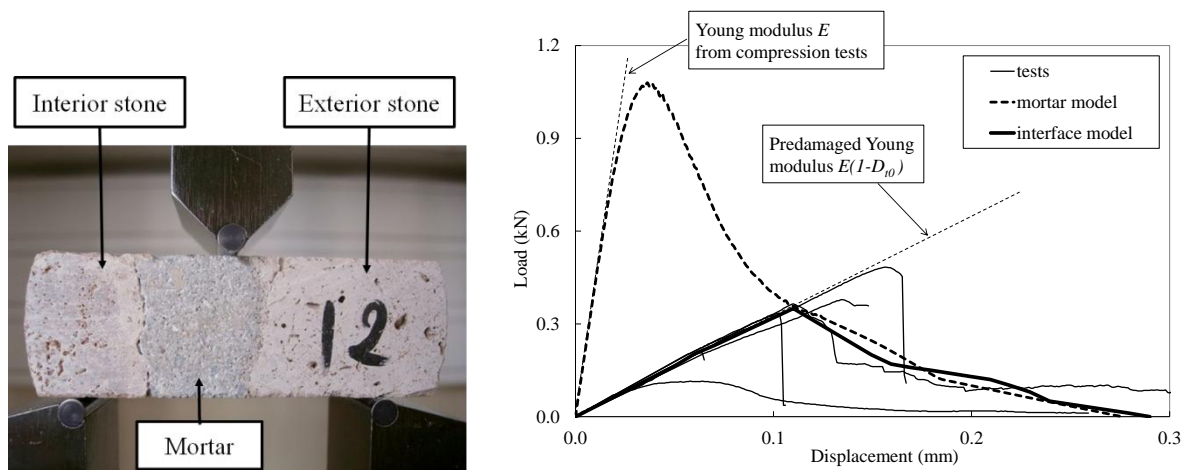


Fig. 13. 3-point-bending test on multilayers (left) and damage model of the mortar-stone interface (right)

The parameter  $w_{ref}$  can only be determined by cyclic tension-compression tests, which were not been carried out during this research. So the value adopted for this parameter was the same as for concrete fracture, 10 $\mu$ m [7].

### The back fill

It was forbidden to pierce the water insulation while coring as it prevents water seepage into the vault. For this reason, no samples were collected from the back fill. So no experimental campaign was possible for this part of the bridge. Without any data about the fill, the stiffness of its constitutive material was set arbitrarily. We assumed that the fill acted as a Drucker Prager material with negligible cohesion, negligible tensile strength, and with a compression strength  $f_c$  and a Young's modulus  $E$  equal to half the values for interior stone masonry. Thus, the role of the backfill in the mechanical behaviour of the bridge was simply to transmit railway loading to the masonry (unfavourable assumption), and provide gravity loads (favourable), as demonstrated by Gago *et al.* [26].

## 4. Numerical analysis of the bridge studied

### 4.1. Mesh

The mesh was built in such a way that the final calculation tool could be used for any masonry arch by providing a limited number of geometrical parameters as described in Fig. 14 (A pre-processor was developed to facilitate the data input). The bridge was divided into 5 zones: the vault (interior stone masonry), which was embedded between the two spandrel walls and the two rings (exterior stone masonry), the abutments (interior stone masonry) and the fill (Drucker Prager material with negligible cohesion).

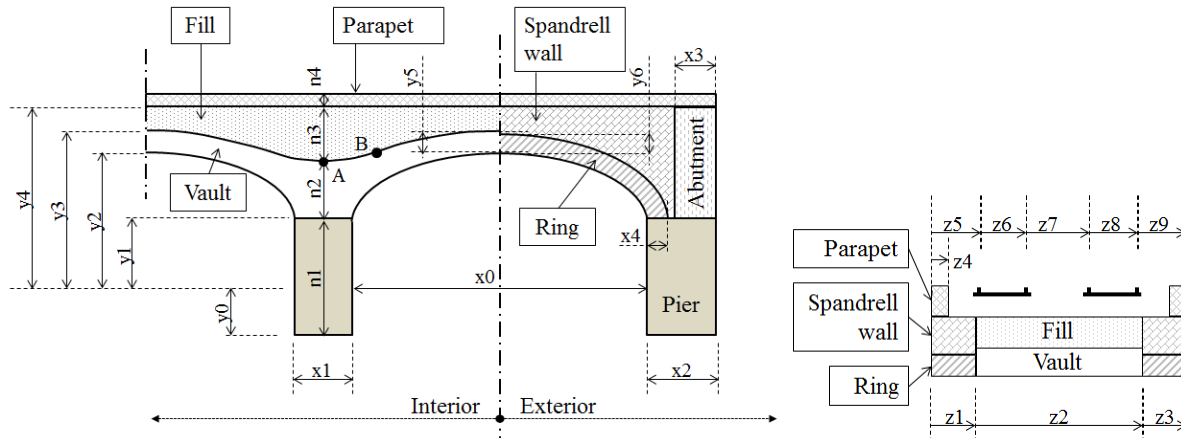


Fig. 14. Geometry of the bridge in the calculation tool

The specific geometry of the Saint Ouen bridge is shown in Fig. 15.

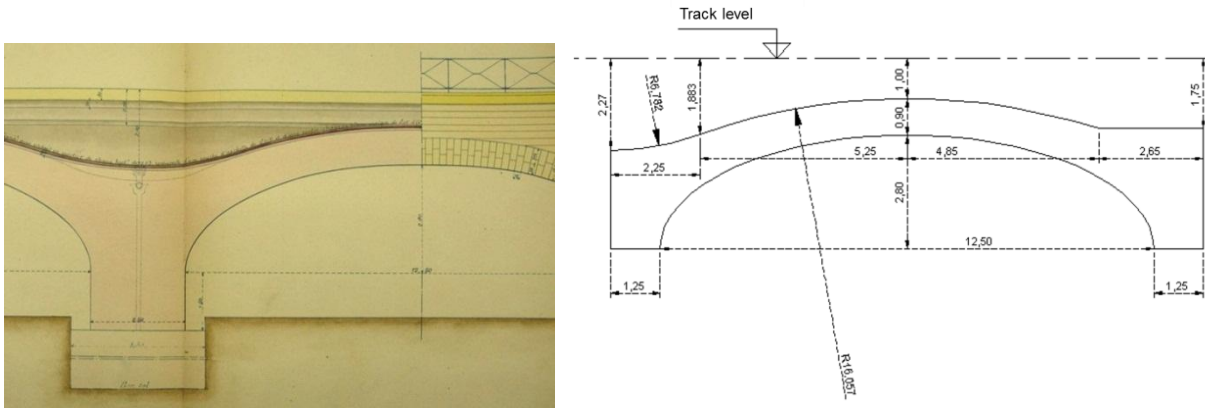


Fig. 15. Geometry of the bridge at Saint Ouen (original outline on the left (1904), layout on the right)

#### 4.2. Boundary conditions

The vertical planes located at each end of the three calculated spans were blocked horizontally in order to simulate the continuum of the bridge symmetrically on each side (Fig. 16).

The soil and foundations under the bridge were modelled by elastic joint elements, the rigidity of which was calculated with respect to the results of the on-site investigations (displacements of pile bases under freight train loads) described in 2.2.3. A first calculation of the bridge determined the rigidity of the foundations such that their vertical displacement under the freight train reached the mean value measured (0.22mm). The foundation rigidity was  $k_n=75\text{MPa/m}$ .

The railway tracks and their support system were added on to the bridge in the form of 4 lines by means of beam elements with an elastic linear law ( $E = 30\text{GPa}$ ,  $\nu=0.2$ ), linked to the structure by joint elements (vertical rigidity =  $100\text{MPa/m}$ , longitudinal rigidity =  $1000\text{MPa/m}$ ). To simplify the approach, the beam finite-elements included the railway tracks, the sleepers and the ballast. This approach was adopted by Noorzaei *et al.* [27] for dynamic loading of railway bridges, with an elasto-plastic material. In our case, an elastic model was used for the tracks to avoid the appearance of damaged areas and localization phenomena in this element (which it was not our goal to study here),

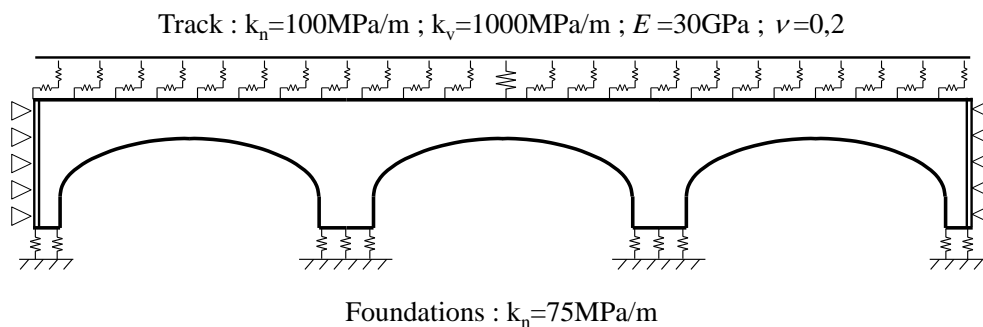


Fig. 16. Location of tracks and loads, boundary conditions

#### 4.3. Calculation method under loads

Three types of actions were considered and applied successively, step by step (Fig. 17): self-weight, displacements of foundations, traffic loads.

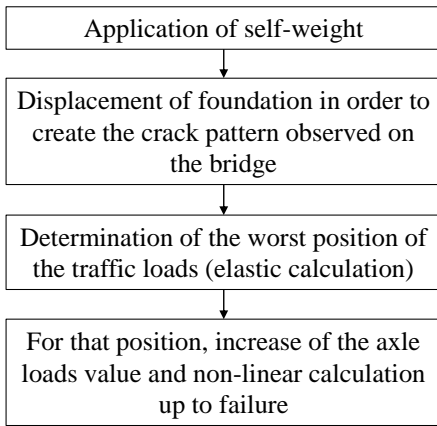


Fig. 17. Calculation steps for the bridge

#### 4.4. Results of calculation

Before any calculations, the pre-damage in tension assessed in 3.2.2 was applied to the whole structure. The material parameters for each zone were those obtained from experimental results by homogenization, as explained in section 3.

##### 4.4.1. Self-weight

Under self-weight, a few very thin cracks appeared symmetrically (Fig. 18). The vault deflection was 2.2cm (point A on Fig. 20).

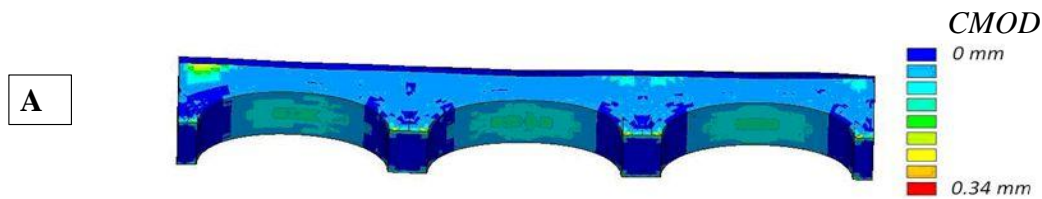


Fig. 18. *CMOD* and cracking scheme under self-weight

##### 4.4.2. Displacements of foundations

In order to create a skew crack opening of 0.7mm under the intrados of the third span as actually observed on the bridge (Fig. 7), differential displacements from 5 to 12cm were applied under the second pile (Fig. 19). Note that these imposed displacements were not measured on site, but fitted to explain the current crack pattern observed (point B on Fig. 20).

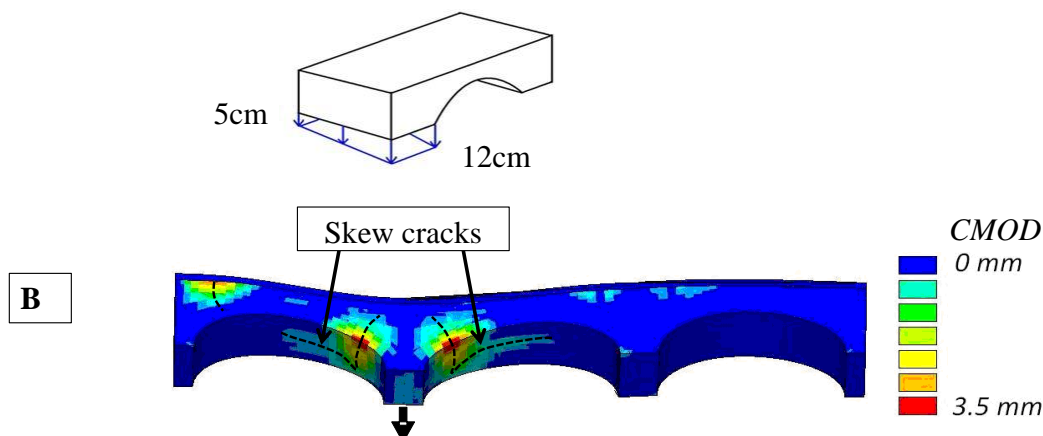


Fig. 19. *CMOD* due to displacements of foundations, applied to create the current cracked state

On Fig. 20, the part of the curve between points 0 and B describes the history of the bridge until today: construction of the masonry on formwork, removal of the formwork, and differential settlements. All these steps are responsible for the current cracked state of the structure. Next, the analysis of the train load effects could be carried out with the real stiffness of this old bridge.

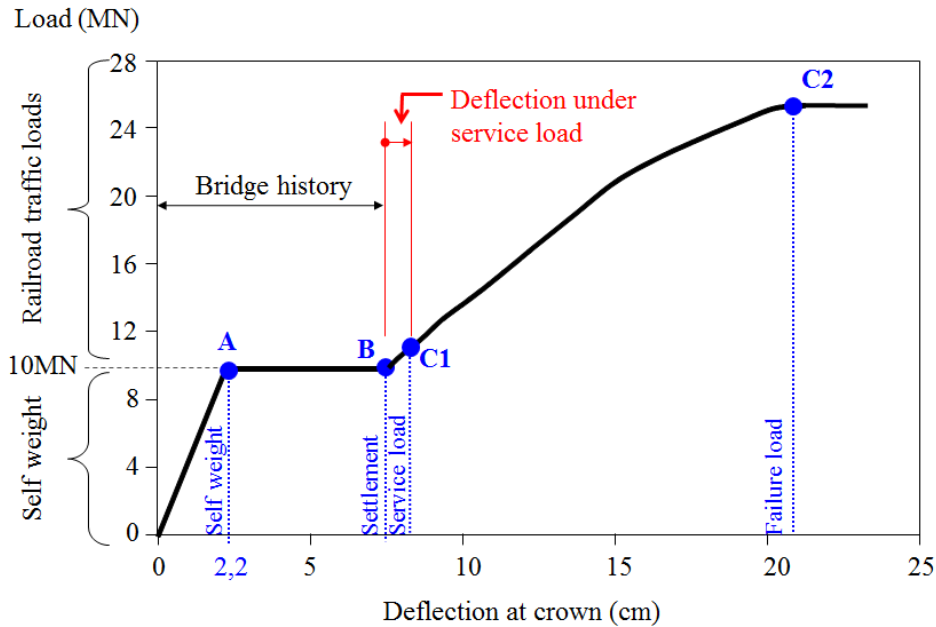


Fig. 20. Deflection of the vault under actions, up to failure

#### 4.4.3. Train load

Finally, a train, represented by a series of axle loads, was applied to the cracked bridge. The worst position of the train (maximum deflection) had been determined in advance by means of a simplified elastic calculation. In that position, the first axle reached around the first third of the central span (top of Fig. 21).

Then, the loads were increased until collapse. On Fig. 20, the real service train is indicated by the point C1. The cracking scheme to collapse is given in Fig. 21. As loads increase, some cracks, in the spandrel walls, reclose. It can be observed that the real train load had no significant effect on the crack opening as measured on site.

The calculation was stopped at failure (25MN, point C2 in Fig. 20), i.e. a train load of 15MN. On the example of Fig. 20, the safety margin between failure load and service load is very high. The bridge studied is very massive and thick. Consequently, below a very high load (around 8MN in this case study), crack propagation did not lead to a sufficient concentration of stress to damage the bridge.

When load increased, a crack propagated near the first support, from the extrados. Progressively, the damaged zone in tension extended towards the intrados (In Fig 21 the compressive zone corresponds to the undamaged parts, and becomes smaller from state C1 to C2). At failure, in the same section, a small zone of the intrados was damaged in compression (Fig. 22). Consequently, a plastic hinge appeared in this section, and failure occurred. Finally, collapse was obtained by the crushing of a block after the occurrence of several stress redistribution mechanisms in the structure. These redistributions were initiated by support settlements and amplified by the propagation of cracks in tension. Therefore, the stress redistribution depended on the ability of the model to capture the crack evolution. In fact, the propagation, opening and reclosure of the cracks decreased the masonry stiffness in tensile zones and, consequently, concentrated stresses in residual compressive zones, finally leading to a crushing of the compressed blocks.

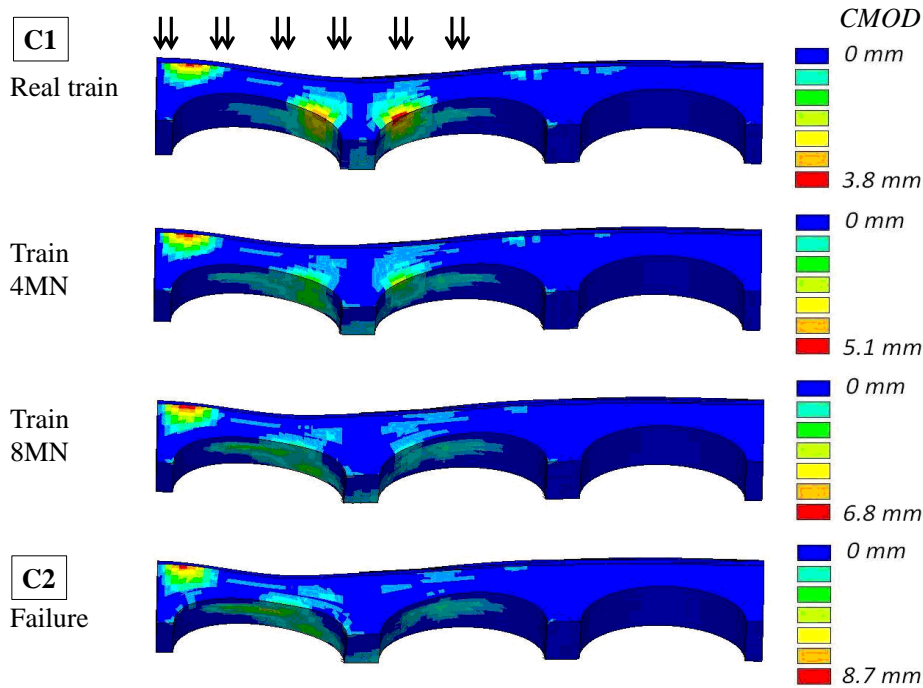


Fig. 21.  $CMOD$  and cracking scheme under train load

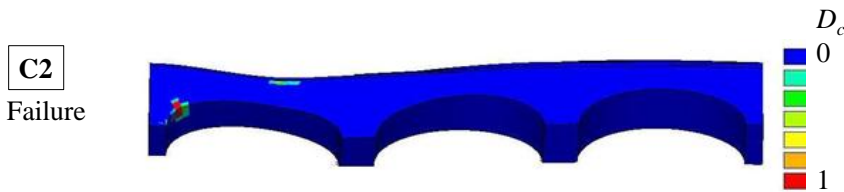


Fig. 22. Damage in compression  $D_c$  at failure

## 5. Conclusion

A mechanical analysis of railway masonry bridges has been presented and applied to the case of a long, multi-span bridge in the suburbs of Paris. It associates in-situ investigations, laboratory tests and a multi-step calculation based on an orthotropic damage model considering crack reclosure possibilities. The damage model includes a treatment of the localization process based on an anisotropic Hillerborgh method and a method to determine  $CMOD$ , the initial value of which can be modified to consider pre-damage in the masonry.

Through the case study, the paper provides a material database of model parameters (except for the backfill), both at the local level (for each individual material) and at the homogenized Representative Volume level. This database could be useful for the analysis of similar old masonry bridges.

The main interest of the case study presented here is to illustrate the global methodology for assessing the mechanical behaviour of old damaged masonry arches. This methodology is able to consider the current disorders of the bridge. It combines the exploitation of the damage model implemented in a FEM code with the results of laboratory tests and in-situ investigations. Because the numerical model is able to simulate an evolving crack pattern, with cracks that can open and reclose in any direction of space, it is possible to find the causes of the disorders

observed in the masonry structure. Thus, the main cracks observed during on-site investigations are explained thanks to a first calculation step, which is a simulation of the bridge history until today. This step mainly concerns the support settlements. Then, the following steps of the calculation, with application of traffic loads, start from a simulated cracking state corresponding to the actual state. It allows the bridge behaviour to be assessed up to failure, which occurs by concentration of compressive stresses in the vault after the tensile cracks have deeply modified the stress distribution. Therefore, the compressive strength of the masonry remains a decisive factor in the load-bearing capacity of the bridge.

The methodology described in this paper is able to consider existing disorders and, consequently, to predict their effects in the presence of various new actions due to, for example, higher traffic loads, increases in train velocity, additional displacement of supports, ballast resurfacing, and widening or reinforcements on the structure.

### Acknowledgements

The technical help and the financial support of the Société Nationale des Chemins de Fer Français (SNCF) and Réseaux Ferrés de France (RFF), granted to the LMDC laboratory for this research, are gratefully acknowledged, specifically M. Plu and M. Dieleman from SNCF's Engineering Division.

### References

- [1] Orbán Z, Gutermann M. Assessment of masonry arch railway bridges using non-destructive in-situ testing methods. *Engineering Structures* 2009;31:2287–98.
- [2] Proske D, Van Gelder P. *Safety of Historical Stone Arch Bridges*. Springer. Springer Berlin Heidelberg; 2009.
- [3] Roca P, Cervera M, Gariup G, Pela L. Structural Analysis of Masonry Historical Constructions. Classical and Advanced Approaches. *Archives of Computational Methods in Engineering* 2010;17:299–325.
- [4] Helmerich R, Niederleithinger E, Trela C, Bień J, Kamiński T, Bernardini G. Multi-tool inspection and numerical analysis of an old masonry arch bridge. *Structure and Infrastructure Engineering* 2012;8:27–39.
- [5] Sellier A, Bary B. Coupled damage tensors and weakest link theory for the description of crack induced anisotropy in concrete. *Engineering Fracture Mechanics* 2002;69:1925–39.
- [6] Sellier A, Casaux-Ginestet G, Buffo-Lacarrière L, Bourbon X. Orthotropic damage coupled with localized crack reclosure processing. Part I: Constitutive laws. *Engineering Fracture Mechanics* 2013;97:148–67.
- [7] Sellier A, Casaux-Ginestet G, Buffo-Lacarrière L, Bourbon X. Orthotropic damage coupled with localized crack reclosure processing. Part II: Applications. *Engineering Fracture Mechanics* 2013;97:168–85.
- [8] Domede N, Sellier A. Numerical analysis of masonry arch bridges : benefits and limits of damage mechanics. ARCH'10, 6<sup>th</sup> International Conference on Arch Bridges, Fuzhou, China: 2010, p. 449–56.

- [9] Domede N, Stablon T, Sellier A. Mechanical analysis of an old masonry bridge in Paris. SAHC12, 8<sup>th</sup> International Conference Structural Analysis of Historical Construction, Wroclaw, Poland: 2012, p. 2162–70.
- [10] Stablon T, Sellier A, Domede N, Plu B, Dieleman L. Influence of building process on stiffness: numerical analysis of a masonry vault including mortar joint shrinkage and crack re-closure effect. *Materials and Structures* 2011;45:881–98.
- [11] Jefferson A. Craft—a plastic-damage-contact model for concrete. I. Model theory and thermodynamic considerations. *International Journal of Solids and Structures* 2003;40:5973–99.
- [12] Stablon T. Méthodologie pour la requalification des ponts en maçonnerie. Université Paul Sabatier, Toulouse 3 - PhD Thesis, 2011.
- [13] Carol I, Rizzi E, Willam K. On the formulation of anisotropic elastic degradation. I. Theory based on a pseudo-logarithmic damage tensor rate. *International Journal of Solids and Structures* 2001;38:491–518.
- [14] Carol I, Rizzi E, Willam K. On the formulation of anisotropic elastic degradation . II . Generalized pseudo-Rankine model for tensile damage. *International Journal of Solids and Structures* 2001;38:519–46.
- [15] Carol I, Rizzi E, Willam K. An “extended” volumetric/deviatoric formulation of anisotropic damage based on a pseudo-log rate. *European Journal of Mechanics - A/Solids* 2002;21:747–72.
- [16] Fichant S, Pijaudier-Cabot G, La Borderie C. Continuum damage modelling: Approximation of crack induced anisotropy. *Mechanics Research Communications* 1997;24:109–14.
- [17] Badel P, Godard V, Leblond J-B. Application of some anisotropic damage model to the prediction of the failure of some complex industrial concrete structure. *International Journal of Solids and Structures* 2007;44:5848–74.
- [18] Pivonka P, Ožbolt J, Lackner R, Mang HA. Comparative studies of 3D-constitutive models for concrete: application to mixed-mode fracture. *International Journal for Numerical Methods in Engineering* 2004;60:549–70.
- [19] Lishak VI, Yagust VI, Yankelevsky DZ. 2-D Orthotropic failure criteria for masonry. *Engineering Structures* 2012;36:360–71.
- [20] Lemaitre J, Chaboche J-L, Benallal A, Desmorat R. *Mécanique des matériaux solides*. Paris: Dunod; 2009.
- [21] Carol I, Rizzi E, Willam K. Discussion on the paper: Application of some anisotropic damage model to the prediction of failure of some complex industrial concrete structure [Pierre Badel, Vincent Godard, Jean-Baptiste Leblond, *Int. J. Solids Struct.* 44 (2007), 5848–5874]. *International Journal of Solids and Structures* 2008;45:4600–2.

- [22] Erdogan F, Sih GC. On the crack extension in plates under plane loading and transverse shear. *Journal of Fluids Engineering* 1963;85:519–25.
- [23] Hillerborg A, Modéer M, Petersson P-E. Analysis of crack formation and crack growth in concrete by means of fracture mechanics and finite elements. *Cement and Concrete Research* 1976;6:773–81.
- [24] Domede N, Sellier A. Experimental and Numerical Analysis of Behaviour of Old Brick Masonries. *Advanced Materials Research* 2010;133-134:307–12.
- [25] Kim JJ, Fan T, Reda Taha MM, Shrive NG. The effect of damage and creep interaction on the behaviour of masonry columns including interface debonding and cracking. *Materials and Structures* 2012;45:15–29.
- [26] Gago AS, Alfaiate J, Lamas A. The effect of the infill in arched structures: Analytical and numerical modelling. *Engineering Structures* 2011;33:1450–8.
- [27] Noorzaei J, Pour PM, Jaafar MS, Fong YC, Thanoon WA-M. Numerical Simulation of Railway Track Supporting System Using Finite-Infinite and Thin Layer Elements Under Impulsive Loads. *Journal of Civil Engineering and Management* 2012;18:245–52.